Manipulation of Airy surface plasmon beams

Felix Bleckmann,[1] Alexander Minovich,[2] Jakob Frohnhaus,[1]
Dragomir N. Neshev,[2] and Stefan Linden[1]

[1] *Physikalisches Institut, Universität Bonn, Nußallee 12, 53115 Bonn, Germany*
[2] *Nonlinear Physics Centre and Centre for Ultrahigh-bandwidth Devices for Optical Systems (CUDOS), Research School of Physics and Engineering, The Australian National University, ACT 0200, Canberra, Australia*

Compiled March 20, 2013

We demonstrate experimentally the manipulation of Airy surface plasmon beams in a linear potential. For this purpose, we fabricate dielectric-loaded plasmonic structures with a graded refractive index by negative-tone grey-scale electron beam lithography. Using such carefully engineered potentials we show that the bending of an Airy surface plasmon beam can be fully reversed by the potential.

OCIS codes: 240.6680, 310.6845, 350.5500

Airy wavepackets and beams [1, 2] have attracted considerable attention with their unique properties: non-diffracting within a diffraction free zone, self-accelerating during propagation, and shape recovering behind obstacles. Since the first experiments the field has experienced a rapid development with the demonstration of, e.g., particle trapping [3], second harmonic generation [4] and plasma generation [5] with Airy beams. Non-paraxial analogues of such beams have been recently demonstrated [6, 7].

Plasmonic Airy beams have also experienced a rapid development with a number of theoretical [8] and experimental studies [9–11]. Potential applications of Airy surface plasmon polaritons (SPPs) are in the fields of plasmonic circuitry [9–11] and hot-spot creation [12] for surface trapping of nano-objects. For such applications, it is strongly desirable to route Airy SPPs along engineered trajectories without disturbing the non-diffracting propagation. This can be achieved by introducing linear potentials along the Airy trajectory [13]. In fact, the non-diffracting nature of Airy wavepackets propagating in a linear potential has already been suggested in Ref. [1] and recently theroretically studied for Airy SPPs propagating in a linear potential formed by a wedged metal-dielectric-metal waveguide [14]. However, the experimental realization of Airy SPP manipulation by a linear potential has remained out of reach, so far.

Here, we experimentally demonstrate the manipulation of the Airy SPP trajectory by a linear potential realized with a wedged dielectric-loaded plasmonic structure. In particular, we demonstrate a complete reversal of the Airy SPP bending, opening new possibilities for engineering the Airy SPP trajectory.

The idea to steer an Airy SPP in a linear potential can be explained by considering a 2D mechanical analogue: Particles are launched with a constant horizontal velocity, $V_x = const$ and vertical velocity depending on the initial particle position, $V_y = B\sqrt{-y_0}$ (B is a positive constant, y_0 is the initial coordinate at $x = 0$) [see Fig. 1(a)]. The path of an Airy SPP [Fig. 1(c)] can be represented by the limiting caustic trajectory of the particle family [red line in Fig. 1(a)], which is parabolic. Applying a constant force F (e.g. gravity) bends the trajectories of the particles along the direction of the force [Fig. 1(b)]. The limiting trajectory of the particle family, however, still remains parabolic. Correspondingly, an Airy SPP also changes its trajectory in a linear potential caused by a linearly graded refractive index. Importantly, the trajectory remains parabolic [Fig. 1(d)] and the beam shape remains constant with propagation. By varying the strength of the linear potential (the gradient of the refractive index) it is then possible to control the trajectory of the Airy SPP [14].

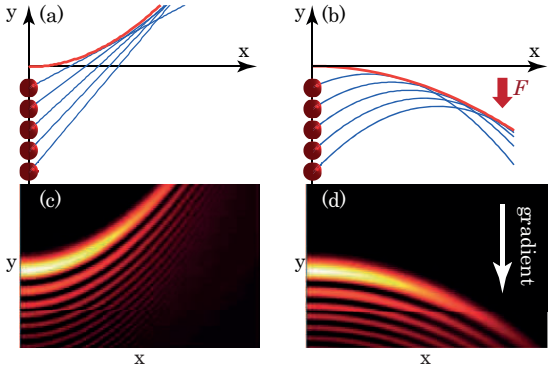

Fig. 1. (Color online) Airy beam manipulation. (a-b) Mechanical analogue of the Airy trajectory. (c-d) Airy beam manipulation in a linear potential (paraxial approximation).

The experimental demonstration of Airy SPP manipulation requires a precise control of the local effective refractive index $n_{\mathrm{eff}}(\mathbf{r})$ of the SPP. It was shown that a dielectric medium deposited on top of a metal modifies the SPP dispersion relation and therefore allows for the local control of the effective refractive index [15–17]. This method has been recently adopted by several groups to demonstrate functional plasmonic elements based on gradient index (GRIN) plasmonics. Devaux *et al.* showed [15] that $n_{\mathrm{eff}}(\mathbf{r})$ can be tailored by locally controlling the effective dielectric constant of the dielectric layer. For this purpose, they decorated a gold film with a varying density of deep sub-wavelength di-

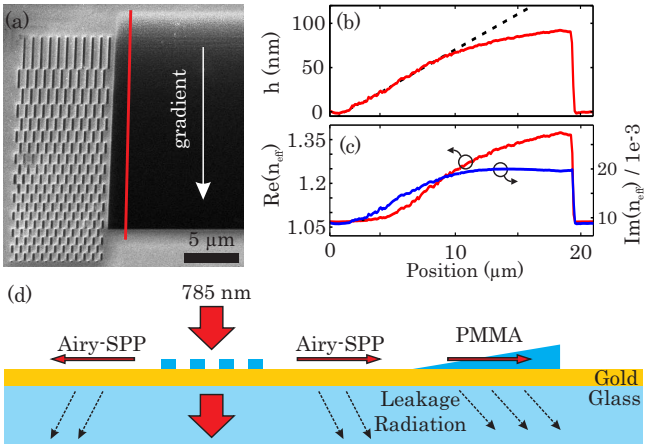

Fig. 2. (Color online) (a) Scanning electron micrograph of a grating coupler for Airy SPPs (left) and a gradient index structure (right). (b) Solid curve: Measured height profile of the gradient index structure. Dashed curve: Height profile used in the numerical calculations.(c) Corresponding profile of the effective refractive index $n_{\text{eff}}(\mathbf{r})$. (d) Schematic of the leakage radiation microscopy setup.

electric protrusions. Alternatively, the SPP dispersion relation can be modified by spatially varying the thickness of a continuous dielectric film deposited on top of a metal film [16, 17]. The latter approach avoids the need for fabrication of deep sub-wavelength features and is therefore less demanding from a fabricational point of view and less prone to scattering losses. The dielectric-loaded plasmonic structures with a spatially variable thickness profile can be fabricated by grey-scale electron beam lithography. For example, this method has been applied to the positive resist polymethyl methacrylate (PMMA) to define plasmonic gradient index elements [17].

Here, we follow a similar approach and use resist structures with a variable thickness profile to control the local effective refractive index $n_{\text{eff}}(\mathbf{r})$ of the Airy SPPs. All functional elements, i.e., the grating coupler as well as the gradient index structure, have been defined by grey-scale electron beam lithography on glass cover slides coated with 1 nm chromium and 60 nm gold. In contrast to Ref. [17], we use PMMA as a *negative-tone resist*. This approach has the advantage that we only expose the areas containing functional elements. By accurate adjustment of the local electron dose, we can continuously vary the thickness h of the cross-linked PMMA resist in the range from $h = 0$ nm to $h \approx 200$ nm.

Figure 2(a) depicts a scanning electron micrograph of a typical sample. It consists of two functional elements: A grating coupler to excite Airy SPPs on the gold-air interface (left hand-side) and a gradient index structure to manipulate the Airy SPP (right hand-side). The design of the grating coupler follows references [9, 12] for a main lobe width $w_0 = 1.0\,\mu$m and has been optimized for the operation wavelength $\lambda = 785$ nm. The elements of the grating have been defined as 100 nm high PMMA slabs. In the same fabrication step we also define the gradient index structure, consisting of a ramp whose thickness increases almost linearly. Its topology as determined by atomic force microscopy is shown in Fig. 2(b). To determine the corresponding effective refractive index profile, we numerically calculate the SPP dispersion relation of a four-layer system consisting of a layer of gold (thickness: 60 nm) and a layer of cross-linked PMMA (thickness: h) sandwiched between a glass and an air half space. The dielectric constants of the four layers were taken as $\epsilon_{\text{Au}} = -19.15 + 2.03\imath$, $\epsilon_{\text{PMMA}} = 2.56$, $\epsilon_{\text{Glass}} = 2.25$ and $\epsilon_{\text{Air}} = 1.0$, respectively. Fig. 2(c) depicts the resulting real and imaginary part of n_{eff} as a function of position. Note, that the dielectric constant of PMMA is assumed to be slightly larger than the literature value ($\epsilon_{\text{PMMA,lit}} = 2.22$) to account for the modification of PMMA due to cross-linking caused by negative-tone grey-scale lithography.

The samples have been optically characterized with a leakage radiation microscopy setup [18] [see Fig. 2(d)]. To launch the Airy SPPs on the gold-air interface, a TM polarized laser beam with 785 nm wavelength has been focused on the grating coupler. As the Airy SPP propagates, a fraction of the SPP leaks through the gold film and couples to radiating modes in the glass substrate. This leakage radiation (as well as the directly transmitted laser beam) has been collected with an oil immersion objective (100×, numerical aperture NA = 1.49) and imaged onto a CCD camera.

Figure 3(a) depicts an experimental leakage radiation microscopy image of the sample displayed in Fig. 2(a). To the left, the Airy SPP propagates along the unstructured gold film. Its main lobe follows a curved trajectory and bends upwards. The presence of the PMMA ramp on the right hand-side of the grating significantly modifies the curvature of the trajectory. Here, we observe a downward bending of the main lobe inside the ramp. This behavior is a result of two counteracting effects. The gradient of $Re(n_{\text{eff}})$ acts as a linear potential that bends the trajectory in the direction of the gradient, i.e., downwards. In contrast, the gradient of $Im(n_{\text{eff}})$ causes an asymmetry of the Airy SPP lobes that moves the maxima of the lobes opposite to the loss gradient [14], i.e., upwards. We can thus conclude that the bending of the trajectory is dominated by the gradient of $Re(n_{\text{eff}})$. However, stronger losses inside of the ramp reduce the propagation length.

We compare our experiments with numerical calculations of the four layer system based on the commercial FDTD software Rsoft. The ramp is approximated by a wedge with linear height gradient $\Delta\text{height}/\Delta\text{position} = 0.008$ which is a good approximation for the first part of the ramp [see dashed line in Fig. 2(b)]. The optical properties of the materials are described with the the dielectric constants stated above. The Airy SPPs are excited with a plane wave source located 400 nm above the metal surface. The source stretches across the whole computational domain in y direction and ends 0.8 μm behind the last PMMA slab in x direction. Due to mem-

ory limitations we calculate the ramp and the bare metal film separately and stitch them afterwards. The resulting square modulus of the total electric field distribution ($|E|^2$) taken at a distance of 10 nm above the metal film is shown in Fig. 3(b). Here, we use different color scales for the left and right parts (ramp part is brightened) to compensate for the fact that in the experiment the dielectric wedge confines SPPs tighter to the interface which is accompanied with an enhancement of the leakage radiation intensity.

The overall agreement between experiment and calculation is very good. Deviations can be mostly traced to the fact that the leakage radiation microscopy image is taken from the glass side of the sample while the electric field is calculated slightly above the metal surface, i.e., where the SPP is actually concentrated. This explains for example why the interference fringes appear in the experimental images while there are absent in the simulations. In the experiment, the fringes result from the interference of the leakage radiation and the exciting laser beam. The period of the interference pattern corresponds to the SPP wavelength.

The curvature of the Airy SPP can be controlled via the slope of the PMMA gradient index structure. In Fig. 3(c), we depict extracted trajectories for two different PMMA ramps with gradients 0.008 and 0.011, respectively, as well as for the bare gold film. As expected, we observe a stronger bending of the trajectory in the case of the larger gradient.

In conclusion, we have demonstrated experimentally and numerically the manipulation of Airy SPPs by a linear potential induced by a wedged dielectric layer on top of a gold film. Our results on reversing the Airy SPP trajectory show that GRIN plasmonics is a powerful method to control the non-diffracting propagation of Airy SPPs. By this approach it will be possible to adapt many functional elements from normal optics to Airy SPPs.

We acknowledge support from the Australian Research Council and the Australian National Computational Infrastructure. Furthermore we thank Bert Kann for the deposition of our gold films.

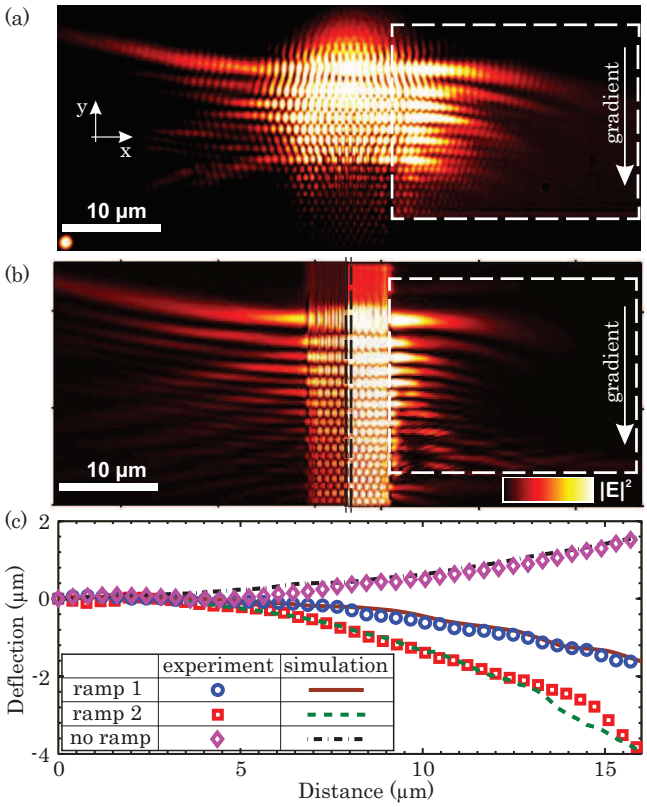

Fig. 3. (Color online) (a) Experimental leakage radiation microscopy image of the sample depicted in Fig. 2(a). (b) Corresponding calculated electric field distribution ($|E|^2$) 10 nm above the metal film. (c) Extracted Airy SPP trajectories for two ramps (gradients 0.008 and 0.011) as well as the bare gold film. The dashed rectangles in (a) and (b) outline the positions of the ramps.

References

1. M. V. Berry and N. L. Balazs, Am. J. Phys. **47**, 264 (1979).
2. G. A. Siviloglou, J. Broky, A. Dogariu, and D. N. Christodoulides, Phys. Rev. Lett. **99**, 213901 (2007).
3. J. Baumgartl, M. Mazilu, and K. Dholakia, Nat. Photon. **2**, 675–678 (2008).
4. T. Ellenbogen, N. Voloch-Bloch, A. Ganany-Padowicz, and A. Arie, Nat. Photon. **3**, 395–398 (2009).
5. P. Polynkin, M. Kolesik, J. V. Moloney, G. A. Siviloglou, and D. N. Christodoulides, Science **324**, 229–232 (2009).
6. P. Zhang, Y. Hu, T. Li, D. Cannan, X. Yin, R. Morandotti, Z. Chen, and X. Zhang, Phys. Rev. Lett. **109**, 193901 (2012).
7. P. Aleahmad, M.-A. Miri, M. S. Mills, I. Kaminer, M. Segev, and D. N. Christodoulides, Phys. Rev. Lett. **109**, 203902 (2012).
8. A. Salandrino and D. N. Christodoulides, Opt. Lett. **35**, 2082 (2010).
9. A. Minovich, A. E. Klein, N. Janunts, T. Pertsch, D. N. Neshev, and Y. S. Kivshar, Phys. Rev. Lett. **107**, 116802 (2011).
10. P. Zhang, S. Wang, Y. Liu, X. Yin, C. Lu, Z. Chen, and X. Zhang, Opt. Lett. **36**, 3191 (2011).
11. L. Li, T. Li, S. M. Wang, C. Zhang, and S. N. Zhu, Phys. Rev. Lett. **107**, 126804 (2011).
12. A. E. Klein, A. Minovich, M. Steinert, N. Janunts, A. Tünnermann, D. N. Neshev, Y. S. Kivshar, and T. Pertsch, Opt. Lett. **37**, 3402–3404 (2012).
13. N. K. Efremidis, Opt. Lett. **36**, 3006–3008 (2011).
14. W. Liu, D. N. Neshev, I. V. Shadrivov, A. E. Miroshnichenko, and Y. S. Kivshar, Opt. Lett. **36**, 1164 (2011).
15. E. Devaux, J. Y. Laluet, B. Stein, C. Genet, T. Ebbesen, J. C. Weeber, and A. Dereux, Opt. Express **18**, 20610 (2010).
16. Y. Liu, T. Zentgraf, G. Bartal, X. Zhang, Nano Lett. **10**, 1991 (2010).
17. T. Zentgraf, Y. Liu, M. H. Mikkelsen, J. Valentine, X. Zhang, Nat. Nanotech. **6**, 151 (2011).
18. A. Drezet, A. Hohenau, D. Koller, A. Stepanov, H. Ditlbacher, B. Steinberger, F. R. Aussenegg, A. Leitner, J. R. Krenn, Mater. Sci. Eng. **B 149**, 220 (2008).

Informational Fourth Page

References with titles

1. M. V. Berry and N. L. Balazs, "Nonspreading wave packets," Am. J. Phys. **47**, 264 (1979).

2. G. A. Siviloglou, J. Broky, A. Dogariu, and D. N. Christodoulides, "Observation of Accelerating Airy Beams," Phys. Rev. Lett. **99**, 213901 (2007).

3. J. Baumgartl, M. Mazilu, and K. Dholakia, "Optically mediated particle clearing using Airy wavepackets," Nat. Photon. **2**, 675–678 (2008).

4. T. Ellenbogen, N. Voloch-Bloch, A. Ganany-Padowicz, and A. Arie, "Nonlinear generation and manipulation of Airy beams," Nat. Photon. **3**, 395–398 (2009).

5. P. Polynkin, M. Kolesik, J. V. Moloney, G. A. Siviloglou, and D. N. Christodoulides, "Curved Plasma Channel Generation Using Ultraintense Airy Beams," Science **324**, 229–232 (2009).

6. P. Zhang, Y. Hu, T. Li, D. Cannan, X. Yin, R. Morandotti, Z. Chen, and X. Zhang, "Nonparaxial Mathieu and Weber Accelerating Beams," Phys. Rev. Lett. **109**, 193901 (2012).

7. P. Aleahmad, M.-A. Miri, M. S. Mills, I. Kaminer, M. Segev, and D. N. Christodoulides, "Fully Vectorial Accelerating Diffraction-Free Helmholtz Beams," Phys. Rev. Lett. **109**, 203902 (2012).

8. A. Salandrino and D. N. Christodoulides, "Airy plasmon: a nondiffracting surface wave," Opt. Lett. **35**, 2082 (2010).

9. A. Minovich, A. E. Klein, N. Janunts, T. Pertsch, D. N. Neshev, and Y. S. Kivshar, "Generation and Near-Field Imaging of Airy Surface Plasmons," Phys. Rev. Lett. **107**, 116802 (2011).

10. P. Zhang, S. Wang, Y. Liu, X. Yin, C. Lu, Z. Chen, and X. Zhang, "Plasmonic Airy beams with dynamically controlled trajectories," Opt. Lett. **36**, 3191 (2011).

11. L. Li, T. Li, S. M. Wang, C. Zhang, and S. N. Zhu, "Plasmonic Airy Beam Generated by In-Plane Diffraction," Phys. Rev. Lett. **107**, 126804 (2011).

12. A. E. Klein, A. Minovich, M. Steinert, N. Janunts, A. Tünnermann, D. N. Neshev, Y. S. Kivshar, and T. Pertsch, Opt. Lett. **37**, 3402–3404 (2012).

13. N. K. Efremidis, "Airy trajectory engineering in dynamic linear index potentials," Opt. Lett. **36**, 3006–3008 (2011).

14. W. Liu, D. N. Neshev, I. V. Shadrivov, A. E. Miroshnichenko, and Y. S. Kivshar, "Plasmonic Airy beam manipulation in linear optical potentials," Opt. Lett. **36**, 1164 (2011).

15. E. Devaux, J. Y. Laluet, B. Stein, C. Genet, T. Ebbesen, J. C. Weeber, and A. Dereux, "Refractive micro-optical elements for surface plasmons: from classical to gradient index optics," Opt. Express **18**, 20610 (2010).

16. Y. Liu, T. Zentgraf, G. Bartal, X. Zhang, "Transformational Plasmon Optics," Nano Lett., **10** 1991 (2010).

17. T. Zentgraf, Y. Liu, M. H. Mikkelsen, J. Valentine, X. Zhang, "Plasmonic Luneburg and Eaton lenses," Nat. Nanotech. **6**, 151 (2011).

18. A. Drezet, A. Hohenau, D. Koller, A. Stepanov, H. Ditlbacher, B. Steinberger, F. R. Aussenegg, A. Leitner, J. R. Krenn, "Leakage radiation microscopy of surface plasmon polaritons," Mater. Sci. Eng. **B 149**, 220 (2008).